arXiv:1612.01161v2 [cond-mat.mes-hall] 6 Dec 2016

Ultrafast ballistic diffusion of nanotubular water shells in carbon nanotubes. Direct experimental evidence with two-dimensional ($D-T_2$) NMR

J. Hassan,[1,*] G. Diamantopoulos,[1] L. Gkoura,[2] M. Karayanni,[2] S. Alhassan,[3] M. S. Katsiotis,[3] T. Karagiannis,[3] M. Fardis,[2] N. Panopoulos,[2] H. J. Kim,[4] and G. Papavassiliou[2,†]

[1]*Department of Applied Math and Sciences, Khalifa University, 127788, Abu Dhabi, UAE*
[2]*Institute of Nanoscience and Nanotechnology, NCSR Demokritos, 15310 Aghia Paraskevi, Attiki, Greece*
[3]*Department of Chemical Engineering, Petroleum Institute, 2533, Abu Dhabi, UAE*
[4]*Nano-Bio Electron Microscopy Research Group, Korea Basic Science Institute, 169-148, Daejeon 305-806, Republic of Korea*

(Dated: December 7, 2016)

Water when confined at the nanoscale acquires extraordinary transport properties. And yet there is no direct experimental evidence of these properties at nanoscale resolution. Here, by using 2D NMR diffusion-relaxation ($D-T_2$) spectroscopy, we acquire the diffusion profile of water in single and double-walled carbon nanotubes (CNTs). Remarkably, in double-walled CNTs water is shown to split in two axial components with the inner one acquiring astonishing flow properties: high fragility, ultra-high self-diffusion coefficient, and "rigid" molecular environment, revealing a nonuniform ballistic mechanism underlying fast diffusion in hydrophobic nanochannels.

PACS numbers: 88.30.rh, 89.40.Cc, 66.10.cg, 68.35.Fx, 82.56.Fk, 47.56.+r

Molecular dynamics (MD) simulations have shown that water in very narrow sub-nanometer CNT channels forms an ordered one-dimensional chain, which spontaneously fills the hydrophobic CNT channels [1]. The estimated flow rates are comparable to those observed in biological pores such as aquaporin, gramicidin, and bacteriorhodosin [2–4]. Other MD simulations have shown that by increasing the CNT diameter nanotube water forms ice nanotubes comprised of a rolled sheet of cubic ice [5], while by further increasing the CNT diameter water is organized in a stratified nanotubular structure with a "chain"-like water component at the center of the CNTs [6–9]. This intriguing molecular arrangement is central in explaining fast water diffusion in CNTs [10], which according to MD simulations takes place either in the form of a single file [11], where water molecules are prevented to surpass each other due to space limitation, or in a ballistic way where clusters of hydrogen bonded water molecules are diffusing very fast in a highly coordinated way [1, 12]. However, MD simulations are strongly model-depending and the true molecular mechanism of the enhanced fluidity is still unclear. Here, on the basis of ^{1}H Nuclear Magnetic Resonance (NMR) diffusion-relaxation ($D-T_2$) spectroscopy we acquire experimentally for the first time the diffusion profile of water in single and double-walled CNTs at nanoscale resolution. Experiments unveil a novel stratified ballistic mechanism as the dominant mechanism of ultrafast water diffusion in narrow CNTs.

Figure 1 summarizes the main results of the present work. In single-walled CNTs (SWCNTs) with inner diameter $d \approx 1.2$ nm NMR experiments show the presence of a single nanotube water component with self-diffusion coefficient D comparable to that of free water. Remarkably, in double-walled CNTs (DWCNTs) with inner diameter ≈ 3.5 nm a second water component is observed with strikingly high D-values, approximately four times higher than that of bulk water at 285 K. The intensity of the NMR signals of the two water components correlates excellently with the radial water density distribution in DWCNTs (green line plot in Figure 1b) from MD simulations [6, 7], as shown below. These results are in agreement with theoretical calculations, which predict that in ultra-narrow CNTs nanotube water diffuses in the shape of hollowed nanotubular clusters with a ballistic-type mechanism [9, 12].

Figure 1c shows the inverse of the measured self-diffusion coefficient, $1/D$ vs. $1000/T$ of nanotube water in both CNTs together with that of bulk water (black circles). This kind of diagrams are very useful in understanding the way that intermolecular interactions propagate in freezing liquids. The blue line is the theoretical simulation of an ideal "strong" liquid with $1/D$ exhibiting Arrhenius temperature dependence, $\frac{1}{D} \propto exp\left(\frac{U}{k_B T}\right)$. As expected, bulk water deviates significantly from the Arrhenius behavior; within Angels concept of fragility [13] bulk water is considered to be fragile [14, 15], i.e. it slows down gradually by cooling and freezes rapidly only near the water glass transition temperature T_g. The black line is theoretical fit to the empirical formula $\frac{1}{D} \propto \frac{1}{D_0}\left(\frac{T-T_S}{T_S}\right)^{\gamma}$ which is widely used in the literature to fit the non-Arrhenius temperature dependence of the water transport properties [13]. T_S in the formula is related to the glass transition temperature T_g. Data are excellently fitted with $\gamma \approx 2$ and $T_S \approx 215$ K, in agreement with previous reported values [16]. In the case of SWCNTs, the $1/D$ values of nanotube water matches excellently with those of bulk water. Most important, in DWCNTs the central water component (cyan spheres in Figure 1b) acquires extremely low $1/D$ values ($\gamma \approx 3$ and $T_S \approx 218$ K), which vary slowly by decreasing temper-

ature, indicating that the water structure of the central water component is robust upon cooling [6, 17]. The robustness of the nanotube water structure is further confirmed in Figure 1d, which presents the ^{1}H NMR spin-lattice to spin-spin relaxation $T_1 - T_2$ correlation spectrum of water in DWCNTs at room temperature. Nanotube water, interstitial water, and free bulk water are easily discriminated in the spectrum, according to their T_2/T_1 ratio [18]. In case of nanotube water, the very low $T_2/T_1 << 1$ ratio is clear evidence that water molecules are in a solid-like than in a liquid-like molecular environment. Evidently, diffusing entities in both CNTs are not single water molecules but nanotubular water clusters diffusing in a ballistic way very fast along the CNTs axis.

2D ($D - T_2$) NMR experiments were performed in

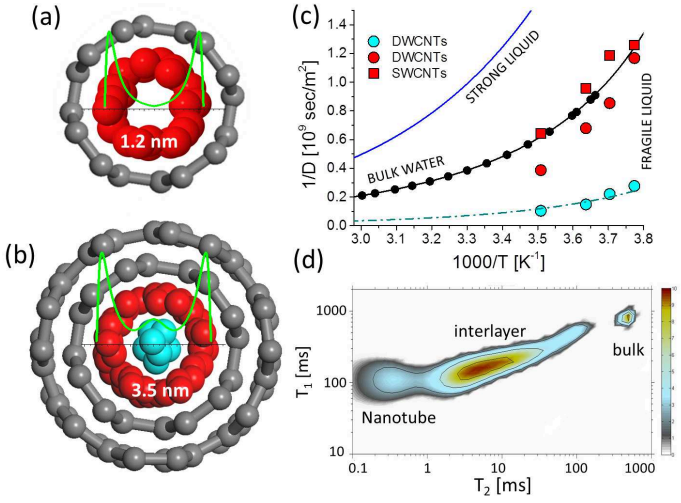

FIG. 1: Schematic presentation of water diffusion in SWCNTs and DWCNTs according to the ^{1}H $D-T_2$ NMR results. The water structure in both SWCNTs (a) and DWCNTs (b) has been sketched by combining the $D - T_2$ NMR results with recent MD simulations [6, 7]. The green plots are sketches of the relevant water density. (c) The inverse of the experimental self-diffusion coefficient $1/D$ as a function of $1000/T$. The blue line shows the temperature dependence of an ideal "strong" liquid following Arrhenius law. The solid black and the dashed cyan lines are theoretical fits as described in the text. (d) ^{1}H NMR spin-lattice to spin-spin relaxation (T_1-T_2) correlation spectroscopy of water saturated DWCNTs in external magnetic field of 9.4 Tesla at room temperature.

the stray field of a superconductive magnet with a constant linear magnetic field gradient $G = 34.7$ Tesla/m. The conventional 1D NMR method for measuring water diffusion in a constant linear magnetic field gradient is to monitor the ^{1}H NMR spin-echo decay and then fitting the obtained decay curve according to relation $M = M_0\, exp\left(-\frac{2\tau}{T_2} - \frac{2}{3}D\gamma^2G^2\tau^3\right)$ where $\gamma = 26.7522$

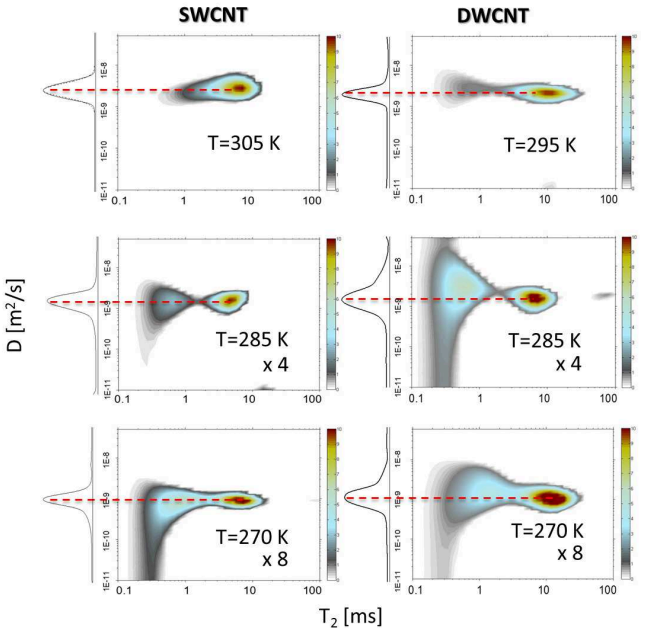

FIG. 2: Contour plots of ^{1}H NMR $D-T_2$ spectra of water in SWCNT (left panel) and DWCNT (right panel) at selected temperatures. Two main components are seen at each temperature, corresponding to nanotube water confined in the CNTs (low T_2 values) and interstitial and bulk water external to the CNTs (high T_2 values). Plots at the left side of the contour plots are the relevant D-projections.

(10^7 rad/sT) is the gyromagnetic ratio for ^{1}H, and D the water self-diffusion coefficient ($D = 2.3 \times 10^{-9}$ m^2/s for bulk water at room temperature). In case of non-uniform diffusion processes with multiple D values, diffusion is expressed with a distribution function $f(D)$, which is obtained by implementing an appropriate "inversion algorithm" [19] as explained in the supplemental material [18]. Furthermore, in case of water diffusion in a bundle of randomly oriented CNTs, $f(D)$ curve acquires a characteristic asymmetric shape with a tail towards low D values, which is the fingerprint of 1D restricted diffusion. It is noticed that ^{1}H NMR studies of water diffusion inside CNTs have been already reported, presenting mainly effective D values [20, 21]. However, it is extremely difficult with conventional 1D NMR diffusion experiments to disentangle water components with relatively close D coefficients, as those encountered in nanotubular channels.

To overcome this obstacle, we take benefit of the fact that nanotube water acquires very short relaxation times. In general, liquids confined in porous structures relax faster than bulk liquids, due to fast exchange between slow relaxing bulk liquid and fast relaxing adsorbed liquid ($T_{2,bulk} >> T_{2,surf}$). In such case, the mean relaxation rate is expressed as $\frac{1}{T_2} \propto k\frac{S}{V}$ where $k = T^{-1}_{2,surf}$ [22]. However, in hydrophobic CNTs water is not in contact with the CNT walls and the short values indicate rather solid-like environment at molecular scale

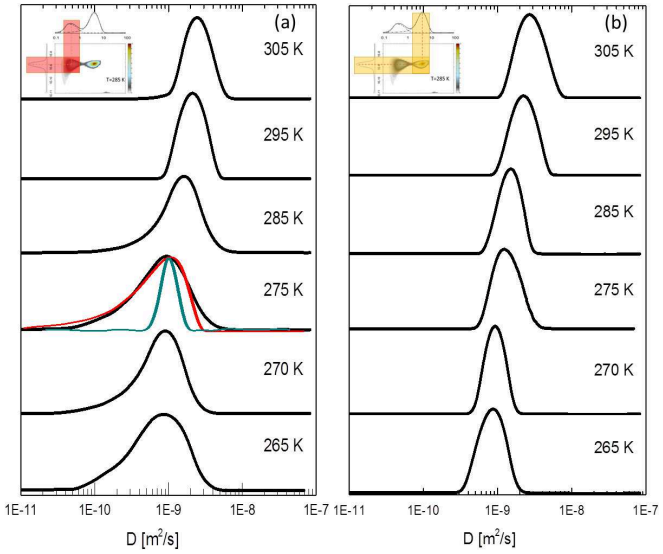

FIG. 3: Fast diffusion of nanotube water in SWCNTs. Self-diffusion coefficient D-projections corresponding solely to (a) nanotube water (shell water) and (b) external water in SWCNT. The insets show the selected areas to acquire the relevant D-projections. For better visualization spectra are normalized to one. For $T < 285$ K projections show a low-D tail, which is characteristic of one-dimensional restricted diffusion. The red line at 275 K is the distribution function $f(D)$ of water diffusing in a bundle of randomly oriented CNTs [18]. The blue line is the relevant simulation to unrestricted diffusion of bulk water.

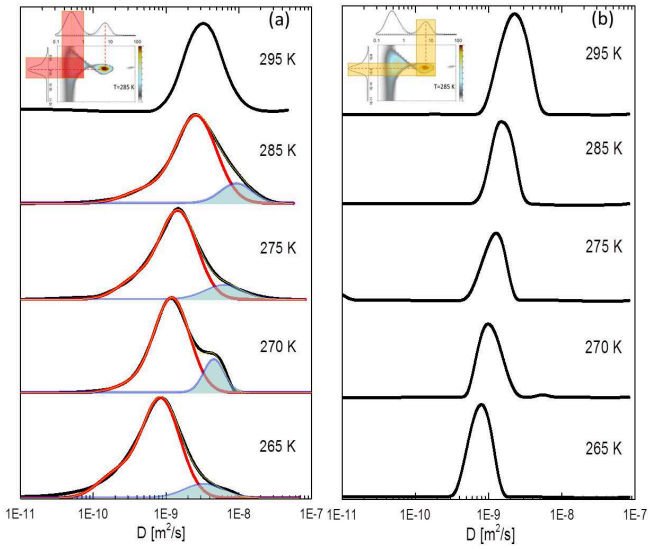

FIG. 4: Stratified fast diffusion of nanotube water in DWCNTs. Self-diffusion coefficient D-projections corresponding solely to (a) nanotube water and (b) external water in DWCNTs. The insets show the selected areas to acquire the relevant D-projections. For better visualization, all plots are normalized to one. For $T < 285$ K projections of nanotube water were fitted with two asymmetric Gaussians. The red colored line corresponds to shell water as in SWCNTs, while the cyan colored line to the axial fast diffusing component at the center of the DWCNTs.

than fast exchange between bulk and adsorbed water molecules. This assumption is confirmed by the very low $T_2/T_1 << 1$ ratio, as shown in the ^{1}H NMR $T_1 - T_2$ spectrum of Figure 1d. The 2D $D - T_2$ results of water in SWCNT and DWCNT are shown in Figure 2 at selected temperatures. Plots were acquired by inversion of the corresponding spin-echo decay curves with a non-negative Tikhonov regularization algorithm [19]. Two main peaks can be observed, corresponding to nanotube water (short T_2 component at ≈ 0.5 ms) and external water (long T_2 component at $\approx 10 - 12$ ms); the former becomes more distinct at temperatures lower than 285 K. Further discussion on the T_2 analysis is presented in the supplemental material [18].

The D projection shown at the left side of the contour plots is what is obtained in a 1D NMR diffusion experiment. Clearly, the D projections have a contribution from both signals (indicated by the horizontal dotted red lines); the diffusion peak from water inside the CNTs is distorted or masked by the signal from the external water. In view of this fact, D projections were calculated separately for each peak and presented in Figure 3 and 4. In both CNTs, external water attains D value $\approx 2.5 \times 10^{-9}$ m^2/s at room temperature, which is very close to that of bulk water. Upon lowering temperature water mobility decreases and the peak shifts to lower D values. At the same time, the intensity of the NMR water signal decreases rapidly. We notice that part of the signal persists even at temperatures lower than the typical freezing point of bulk water (≈ 273 K). Therefore, this signal cannot be assigned to "bulk" water but rather to interstitial water restricted in the space between CNT bundles with molecules possessing liquid-like mobility.

Acquiring D projections solely from nanotube water uncovers important—otherwise not directly accessible—information. In the case of SWCNTs at temperatures below 285 K, D projections exhibit the characteristic low-D tail (Figure 3a), encountered with 1D diffusion in randomly oriented CNTs [23]. This is manifested with the theoretical red line (details are presented in the supplementary information [18]), which simulates accurately the experimental spectrum in the left panel of Figure 3 at a temperature of 275 K. The theoretical model refers to water diffusion in a randomly oriented array of CNT tubes with short (nanometer scale) inner radial dimension but long (micrometer scale) axial dimension, with a single D-value. Impressively, the restricted diffusion in SWCNTs acquires D values close to that of free water, as presented in Figure 1c, in agreement with MD calculations [24].

In the case of DWCNTs, the D-values distribution of water inside the CNTs attains a more intriguing picture. At $T = 285$ K, diffusion of nanotube water is ob-

served to be resolved in two components with peaks centered at $D \approx 2.58 \times 10^{-9}$ m^2/s, and 9.60×10^{-9} m^2/s (Figure 4a). This is in agreement with MD simulations [24], which show that by increasing the CNTs diameter, a stratified arrangement of water molecules takes place [6, 7, 25]. The split of water in two components is explainable by considering repulsive Coulomb forces [26] between next neighboring oxygen atoms, which become important when water is squeezed into narrow hydrophobic CNTs. In view of these facts water inside DWCNTs is considered to be organized in two axial water components as shown in Figure 1a, with the inner one exhibiting astonishing diffusion enhancement, approximately four times higher than that of bulk water at 285 K. Apparently, the lower D value of the outermost axial water component is due to "friction", i.e. interaction of water molecules with defects and oxygen moieties, which unavoidably are present on the CNT walls. Most important, fast diffusion shows up in a rigid molecular environment as witnessed by the very low ^{1}H NMR $T_2/T_1 << 1$ ratio presented in Figure 1d. A similar short T_2/T_1 ratio is observed in SWCNTs. This is evidence that diffusion in narrow CNTs takes place with a ballistic-type mechanism [1, 12] instead of a single-file mechanism [11, 20].

In conclusion, herein we report the first experimental measurement of fast water diffusion in single and double-walled CNTs at nanoscale resolution with a 2D ^{1}H NMR method. It is noticed that the time span of the presented NMR diffusion measurements was $\approx 1 - 2$ ms, i.e. two-to-three orders of magnitude longer than in MD calculations. This allows assessment even of ultra-slow motions of macromolecules, such as those through biological membranes. In DWCNTs water at the center of the nanotubes acquires extraordinary flow properties: high fragility, ultrafast diffusion, and a rigid molecular environment. Combining the NMR experimental results with existing MD calculations, we come to the conclusion that fast diffusion in DWCNTs takes place as random stratified axial motion of water shells with enhanced diffusion at the center, a discovery of significant importance in the efforts to understand fluidic properties through extremely narrow pores and membranes [27, 28], especially of biological interest [29].

ACKNOWLEDGEMENTS

This work was supported by Khalifa University Fund (210065). G.P. and H.J.K. would like also to express their gratitude to IRSES FP7 project Nanomag (295190).

* Corresponding author: Jamal.Hassan@kustar.ac.ae

† Corresponding author: g.papavassiliou@inn.demokritos.gr

[1] G. Hummer, J. C. Rasaiah, and J. P. Noworyta, Nature **414**, 188 (2001).
[2] Y. Kong and J. Ma, Proc. Natl. Acad. Sci. **98**, 14345 (2001).
[3] R. Pomès and B. Roux, Biophys. J. **82**, 2304 (2002).
[4] J. K. Lanyi, J. Phys. Chem. B **104**, 11441 (2000).
[5] K. Koga, G. T. Gao, H. Tanaka, X. C. Zeng, Nature **412**, 802 (2001).
[6] J. R. Bordin, A. Diehl, and M. C. Barbosa, J. Phys. Chem. B **117**, 7047 (2013).
[7] S. Joseph and N. R. Aluru, Nano Lett. **8**, 452 (2008).
[8] A. I. Kolesnikov, J. -M. Zanotti, C. -Z Loong, P. Thiyagarajan, A. P. Moravsky, R. O. Loufty, C. J. Burnham, Phys. Rev. Lett. **93**, 035503 (2004).
[9] A. Striolo, A. A. Chialvo, K. E. Gubbins, and P. T. J. Cummings, J. Chem. Phys. **122**, 234712 (2005).
[10] J. K. Holt, H. G. Park, Y. Wang, et al., Science **312**, 1034 (2006).
[11] A. Kalra, S. Garde, G. Hummer, Proc. Natl. Acad. Sci. **100**, 10175 (2003).
[12] A. Striolo, Nano Lett. **6**, 633 (2006).
[13] R. Speedy and C. Angell, J. Chem. Phys. **65**, 851 (1976).
[14] F. X. Prielmeier, E. W. Lang, R. J. Speedy, and H. D. Lüdemann, Phys. Rev. Lett. **59**, 1128 (1987).
[15] A. Dehaoui, B. Issenmann, and F. Caupin, Proc. Natl. Acad. Sci. **112**, 12020 (2015).
[16] F. Perakis, P. Hamm, J. Phys.Chem. B **115**, 5289 (2011).
[17] N. Mauro, M. Blodgett, M. L. Johnson, A. J. Vogt, and K. Kelton, Nat. Commun. **5**, 4616 (2014).
[18] See Supplemental Material at [URL] for detailed description of the applied two dimensional NMR methods and the ^{1}H NMR relaxation study of water in CNTs.
[19] J. Mitchell, T. C. Chandrasekera, and L. F. Gladden, Prog. Nucl. Magn. Reson. Spectrosc. **62**, 34 (2012).
[20] A. Das, S. Jayanthi, H. S. M. V. Deepak, K. V. Ramanathan, A. Kumar, C. Dasgupta, and A. K. Sood, ACS Nano **4**, 1687 (2010).
[21] X. Liu, X. Pan, S. Zhang, X. Han, and X. Bao, Langmuir **30**, 8036 (2014).
[22] J. R. Zimmerman and W. E. Brittin, J. Phys. Chem. **61**, 1328 (1957).
[23] P. T. Callaghan, K. W. Jolley, and J. Lelievre, Biophys. J. **28**, 133 (1979).
[24] A. Alexiadis and S. Kassinos, Chem. Rev. **108**, 5014 (2008).
[25] A. Barati Farimani and N. R. Aluru, J. Phys.Chem. B **115**, 12145 (2011).
[26] T. Head-Gordon and F. H. Stillinger, J. Chem. Phys. **98**, 3313 (1993).
[27] R. Garcia-Fandiño and M. S. P. Sansom, Proc. Natl. Acad. Sci. **109**, 6939 (2012).
[28] J. Geng, K. Kim, J. Zhang, A. Escalada, R. Tunuguntla, L. R. Comolli, F. I. Allen, A. V. Shnyrova, K. R. Cho, D. Munoz, *et al.*, Nature **514**, 612 (2014).
[29] F. Fornasiero, H. G. Park, J. K. Holt, M. Stadermann, C. P. Grigoropoulos, A. Noy, and O. Bakajin, Proc. Natl. Acad. Sci. **105**, 17250 (2008).

Ultrafast ballistic diffusion of nanotubular water shells in carbon nanotubes. Direct experimental evidence with two-dimensional $(D - T_2)$ NMR

J. Hassan,[1,*] G. Diamantopoulos,[1] L. Gkoura,[2] M. Karayanni,[2] S. Alhassan,[3] M. S. Katsiotis,[3] T. Karagiannis,[3] M. Fardis,[2] N. Panopoulos,[2] H.J. Kim,[4] and G. Papavassiliou[2,†]

[1]*Department of Applied Math and Sciences, Khalifa University, 127788, Abu Dhabi, UAE*

[2]*Institute of Nanoscience and Nanotechnology, NCSR Demokritos, 15310 Aghia Paraskevi, Attiki, Greece*

[3]*Department of Chemical Engineering, Petroleum Institute, 2533, Abu Dhabi, UAE*

[4]*Nano-Bio Electron Microscopy Research Group, Korea Basic Science Institute, 169-148, Daejeon 305-806, Republic of Korea*

(Dated: December 7, 2016)

PACS numbers: 88.30.rh, 89.40.Cc, 66.10.cg, 68.35.Fx, 82.56.Fk, 47.56.+r

Keywords: carbon nanotubes, water transportation, self-diffusion in liquids (mass diffusion), diffusion, multidimensional NMR, flows through porous media

arXiv:1612.01161v2 [cond-mat.mes-hall] 6 Dec 2016

In this supplementary information, we provide additional details on certain aspects of the study reported in the manuscript.

The following issues are discussed:

1. Materials and Methods.

2. ^{1}H NMR 2D diffusion - spin-spin relaxation time ($D-T_2$) method in permanent linear magnetic field gradient.

3. ^{1}H NMR diffusionstudy of water in randomly oriented nanochannels.

4. ^{1}H NMR relaxation analysis of water in CNTs.

1. MATERIALS AND METHODS

Purified and open ended carbon nanotubes (SWCNT and DWCNT) were purchased from SES research, USA. The outer diameter of the CNTs used in this work was ≈ 2 nm for the SWCNT and ≈ 5 nm for the DWCNT. Both kinds of CNTs had average length ≈ 1 μm.

Morphological analysis of the carbon nanotubes (CNTs) was performed with Transmission Electron Microscopy (TEM) using a FEI Tecnai G20 microscope with a 0.11 nm point to point resolution, operated at 200 kV. For this analysis, approximately 1 mg of each sample was dispersed in 20 ml of high purity cyclohexane (Merck, 99.9 %) via sonication ($\approx$ 15 s); a drop of each suspension was deposited on copper grids (400 mesh) covered with thin amorphous carbon film (lacey carbon). To avoid contamination, CNT samples were inserted in the TEM machine immediately following preparation. Bright field images were collected at several magnifications in order to observe structure and size homogeneity. Fig. 1 shows representative TEM images of the single walled (SWCNT) and double walled (DWCNT) samples used in this study.

^{1}H NMR two-dimensional diffusion-relaxation (2D $D-T_2$) measurements were performed in the stray field of a 4.7 T Bruker superconductive magnet providing a 34.7 T/m linear magnetic field gradient at ^{1}H NMR frequency of 101.324 MHz. The experiments were carried out by using a pulse sequence with more than 5000 pulses (details are presented below). The sample temperature was controlled by an ITC5 temperature controller in a flow type Oxford cryostat. The accuracy of the temperature was ≈ 0.1 K. An equilibrium time period of about thirty minutes was allowed at each temperature before collecting data.

NMR data were analyzed using a 2D non-negative Tikhonov regularization inversion algorithm code developed by the authors, as discussed below.

In order to prepare fully water saturated samples, CNT powder was immersed in deionized water inside an NMR quartz tube. The sample was then equilibrated at room temperature for a couple of hours. In order to force water to enter the tube (with air extrusion), quartz NMR tubes containing the sample were connected to a vacuum system and carefully pumped out until water immersed in the powder CNTs sample. Each sample was then flame sealed under vacuum with a small layer of free water left on the top of the powder. The same sample preparation procedure was followed for both CNT types used in this study.

2. ^{1}H NMR 2D DIFFUSION-SPIN-SPIN RELAXATION TIME ($D-T_2$) METHOD IN PERMANENT LINEAR MAGNETIC FIELD GRADIENT

Two-dimensional ^{1}H NMR $D-T_2$ was implemented, in order to study water diffusion in single and double walled CNTs. Measurements were performed on a broadband home-built NMR spectrometer operating in the frequency range 5 MHz - 1 GHz. The probe was placed in the fringe field of a 4.7 T Bruker magnet with a linear magnetic field gradient G=34.7 T/m at ^{1}H NMR frequency of 101.324 MHz [1, 2]. The advantage of using a permanent magnetic field gradient instead of a pulsed one, is that (i) G in the fringe field of a superconductive

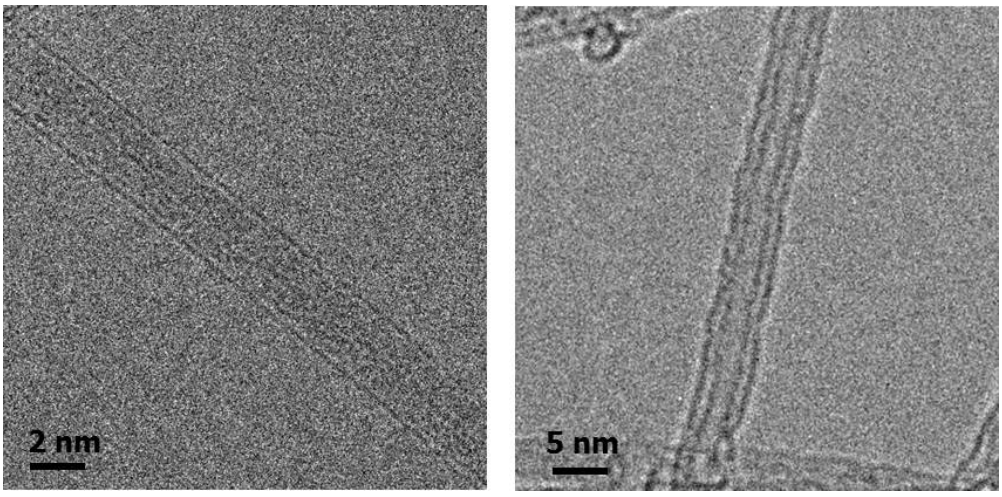

FIG. 1: TEM images for the SWCNT (left) and DWCNT (right) used in this study. The outer diameters of the SWCNT and DWCNT samples were ≈ 2 nm and ≈ 5 nm, respectively.

magnet is very strong, allowing the measurement of very slow diffusion processes (ii) the time between pulses can be set to very short values, due to the absence of pulsed gradient stabilization effects, allowing measurements of very short T_2 values.

The $D-T_2$ pulse sequence is shown in the upper panel of Fig. 2. It consists of a $\pi/2-t_D-\pi$ (Hahn echo) pulse sequence, followed by a train of 5000 π pulses, generating a Carr-Purcell-Meiboom-Gill (CPMG) spin-echo decay (SED) train [3, 4]. The $\pi/2$ pulse duration was set to 4μs and the CPMG interpulse time distance "t" to 30μs. $D-T_2$ data were acquired with a series of 1D experiments. Data in the "direct" (T_2) dimension, were collected in a single shot, by recording simultaneously the intensity of all CPMG echoes. Data in the "indirect" dimension (D) were accumulated in successive experiments by incrementing t_D [3–5]. Fifty experiments were performed with t_D values between 30 μs to 1500 μs in logarithmic scale.

The lower panel in Fig. 2 demonstrates SEDs for three different t_D values. The inset is the signal intensity variation of the first spin-echo as a function of t_D. The solid line in the inset is fit to the relation [1–4]:

$$M = M_0 exp(-\frac{2t_D}{T_2} - \frac{2}{3}\gamma^2 D G^2 t_D^3) \tag{1}$$

In the presence of a broad distribution of diffusion processes and relaxation times, the $D-T_2$ signal intensity decays according to the relation [3, 4]:

$$\frac{g(t_D,t)}{g(0,0)} = \int\int_{-\infty}^{+\infty} (e^{-\frac{DG^2\gamma^2(t_D)^3}{12}} e^{-\frac{t_D}{T_2}}) e^{-\frac{t}{T_2}} f(D,T_2)\, dD\, dT_2 \tag{2}$$

where $f(D,T_2)$ is the distribution function of D and T_2.

For the determination of $f(D,T_2)$ a change of variables was applied [3, 4] $t_t = t + t_D$. This allows separation of the D and T_2 axis, resulting in the following expression:

$$\frac{g(t_D,t)}{g(0,0)} = \int\int_{-\infty}^{+\infty} (e^{-\frac{DG^2\gamma^2(t_D)^3}{12}})(e^{-\frac{t_t}{T_2}}) f(D,T_2)\, dD\, dT_2 \tag{3}$$

The penalty of this transformation is that a small number of echoes at the beginning of the data array is not taken into consideration in the 2D inversion. In this study, the first 100 echoes out of 5000 echoes were excluded, which accounts that NMR signals with T_2 component shorter than ≈ 0.5 ms become invisible.

$D-T_2$ spectra (i.e. the $f(D,T_2)$ distribution function) were obtained using a 2D non-negative Tikhonov regularization algorithm [5, 6] developed in Matlab. In this method

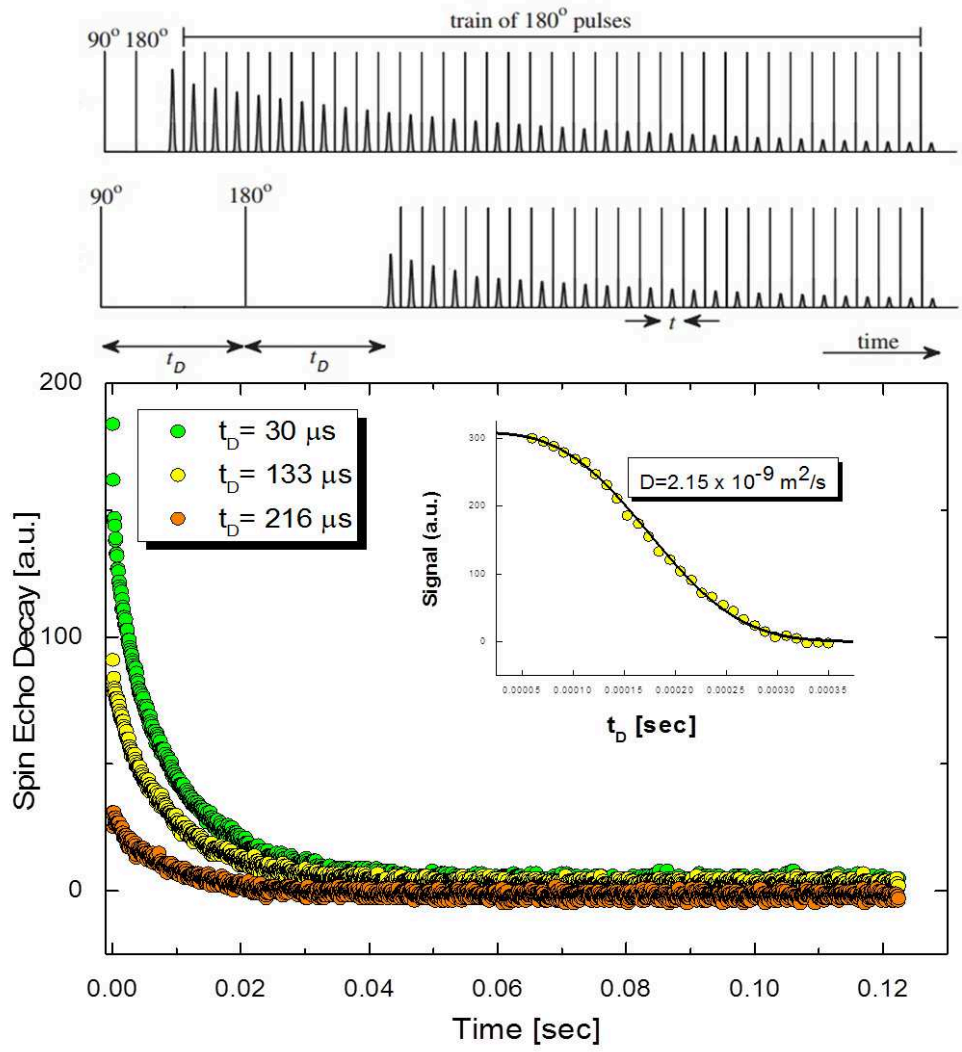

FIG. 2: (Upper panel) The $D-T_2$ NMR pulse sequence. Experiments were operated in a constant linear magnetic field gradient $G = 34.7$ T/m. The signal intensity of the first spin-echo depends on t_D (see inset of the lower panel) according to relation 1S. The CPMG spin-echo decay, following the first echo, provides information on T_2. The "diffusion" axis was scanned with fifty different t_D values ranging from 20 μs to 1000 μs. (Lower panel) CPMG spin-echo decay for the SWCNTs at room temperature, acquired at three different t_D values; 30, 133 and 216 μs. The inset is the decay of the first echo, together with the fit by relation 1S.

2D data are lexicographically transformed in a single column and subsequently inverted by applying a 1D Tikhonov inversion. The inverted data are presented as 1D vector, where the 2D spectrum is encrypted. Unwrapping this again in two dimensions provides the $D-T_2$ spectrum.

3. ^{1}H NMR DIFFUSION STUDY OF WATER IN RANDOMLY ORIENTED NANOCHANNELS

In case of diffusion in a bundle of randomly oriented one-dimensional (1D) nanochannels, relation (1S) describing unrestricted 3D diffusion does not hold anymore, and it should be modified in order to take into account the 1D properties of the system and the random orientation of the nanotubes (in our case CNTs) in respect to the external magnetic field gradient G. This issue was addressed by Callaghan [7], who demonstrated that water diffusion in endosperm tissue of wheat grains, when simulated with diffusion in 1D randomly oriented array of capillaries, averaged over all solid angles, gives spin-echo attenuation R_{1D} according to relation:

$$R_{1D} = \int_0^1 e^{-kDx^2}\, dx \tag{4}$$

For diffusion in the stray field gradient G of the magnet, k is given by $k = \frac{2}{3}\gamma^2 G^2 t_D^3$. The difference in the spin-echo attenuation between unrestricted 3D diffusion and restricted diffusion in 1D is best seen in Fig. 3, which shows the theoretical SED curves acquired by relations (1S) for bulk water diffusion and (4S) for 1D restricted diffusion. While the spin-echo attenuation for unrestricted 3D diffusion decreases "linearly" in the semi-log plot of Fig. 3, the spin-echo intensity of 1D diffusion decreases following a successively declining slope, which by inverting data, gives rise to an asymmetric curve with a long tail towards the low D values (Fig. 4). This is the fingerprint of uniform 1D restricted diffusion in a set of randomly oriented nanochannels.

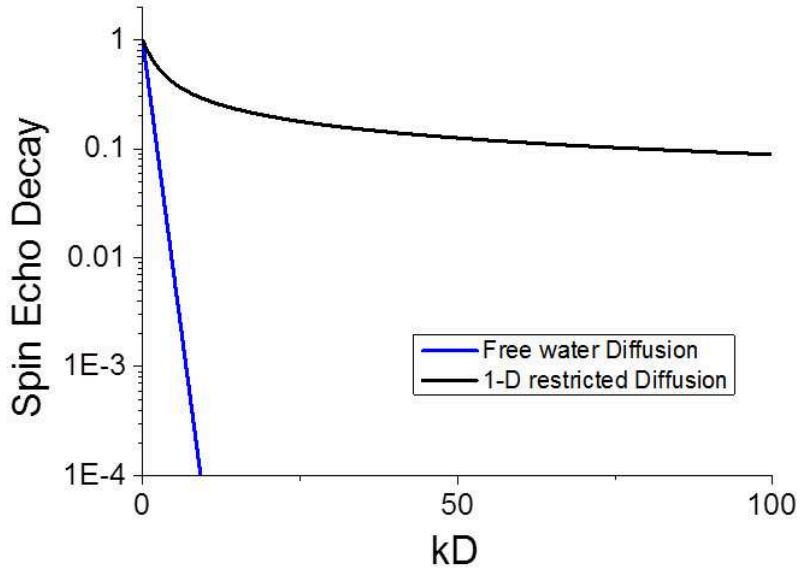

FIG. 3: Theoretical ^{1}H NMR Spin Echo decays of free water molecules (blue line), and water molecules diffusing in one-dimensional randomly oriented nanochannels (black line), where k in the x-axis is equal to $k = \frac{2}{3}\gamma^2 G^2 t_D^3$

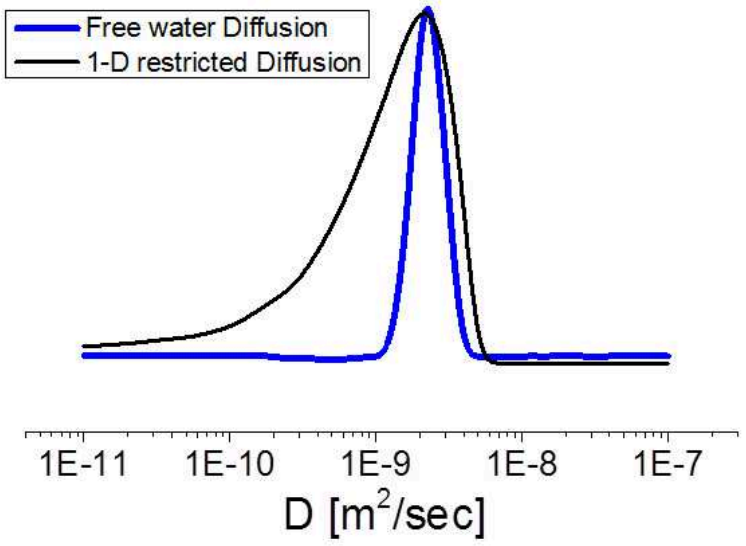

FIG. 4: Self-diffusion coefficient D distribution simulations acquired by implementing a 1D Tikhonov regularization algorithm on the theoretical ^{1}H NMR Spin Echo decays of Fig. 3.

4. ^{1}H NMR RELAXATION ANALYSIS OF WATER IN CNTS

In order to distinguish among the various kinds of water in terms of their dynamics, ^{1}H NMR spin-lattice relaxation T_1 and spin-spin relaxation T_2 measurements were performed in magnetic field 9.4 Tesla (Larmor frequency 400 MHz) and in the stray field of a 4.7 Tesla superconductive magnet at Larmor frequency 101.324 MHz. The main panel in Fig. 5 shows the spin echo decay obtained with a CPMG pulse sequence in field 9.4 Tesla, on a saturated sample of DWCNTs at room temperature. The yellow line is the theoretical fit by implementing a 1D nonnegative Tikhonov regularization algorithm. Gray circles in the inset demonstrate the inverted T_2 distribution. Water is shown to be grouped in two main T_2 peaks; a low intensity narrow peak with $T_2 = 1.2$ sec, corresponding to T_2 values of bulk water, and a second broad line with a peak at 10 msec, which corresponds to interstitial water and water inside the carbon nanotubes. This assignment is confirmed with T_1 measurements (cyan circles), obtained with an inversion recovery $\pi - t - \pi/2$ pulse sequence. According to Fig. 5 T_1 shows two peaks: a peak with T_1 value coinciding with the long T_2 component (as expected for bulk water), and the second one with T_1 value sufficiently higher than the short T_2 component, as expected for interstitial and nanotube water molecules.

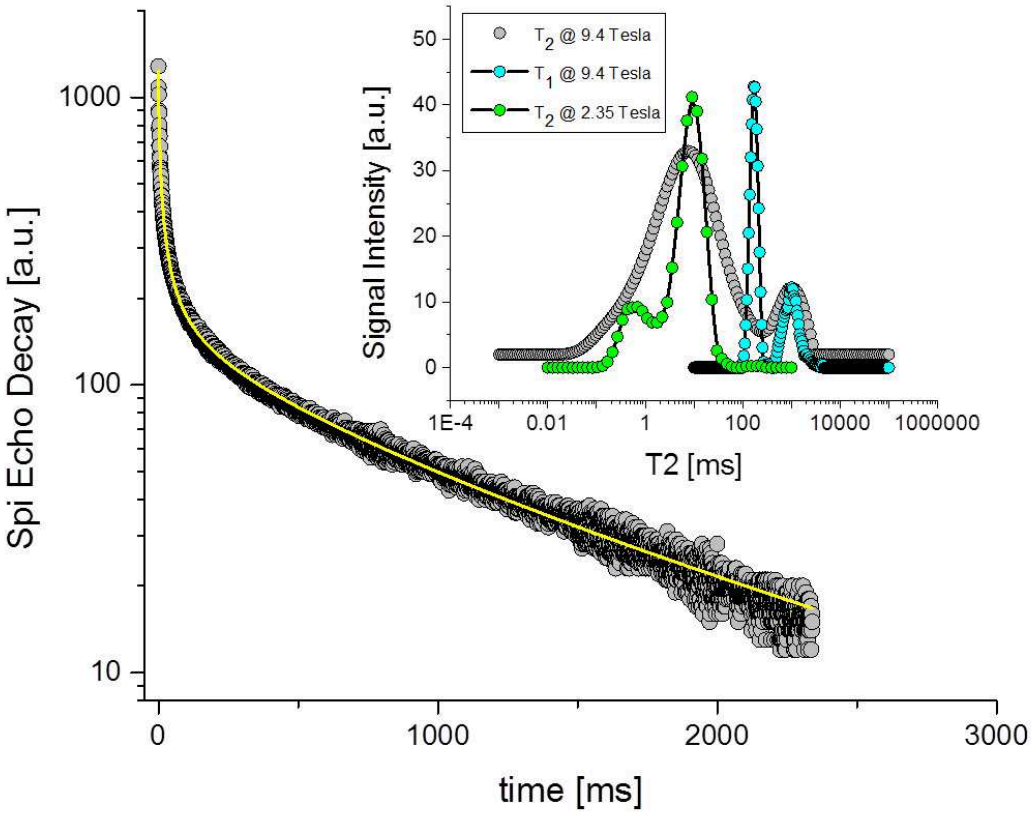

FIG. 5: (Main panel) ^{1}H NMR CPMG spin echo decay of water in a saturated sample of DWCNT at room temperature, in a magnetic field 9.4 Tesla (400 MHz). The yellow line is theoretical fit by applying the 1D Tikhonov regularization inversion. The inset presents the relevant ^{1}H NMR T_2 distribution (gray circles), together with the ^{1}H NMR spin-lattice relaxation time T_1 distribution (cyan circles) and the ^{1}H NMR T_2 distribution of the same sample in the stray field of a 4.7 Tesla (101.324 MHz), green circles.

Most notable, the T_2 projection of the $D-T_2$ plot at 295 K (green circles), coincides with the T_2 distribution of nanotube and interstitial water at 400 MHz (black circles). This is direct evidence that water in the $D-T_2$ measurements is not bulk water but primarily interstitial water (long T_2 component) and nanotube water (short T_2 component), as discussed in the article.

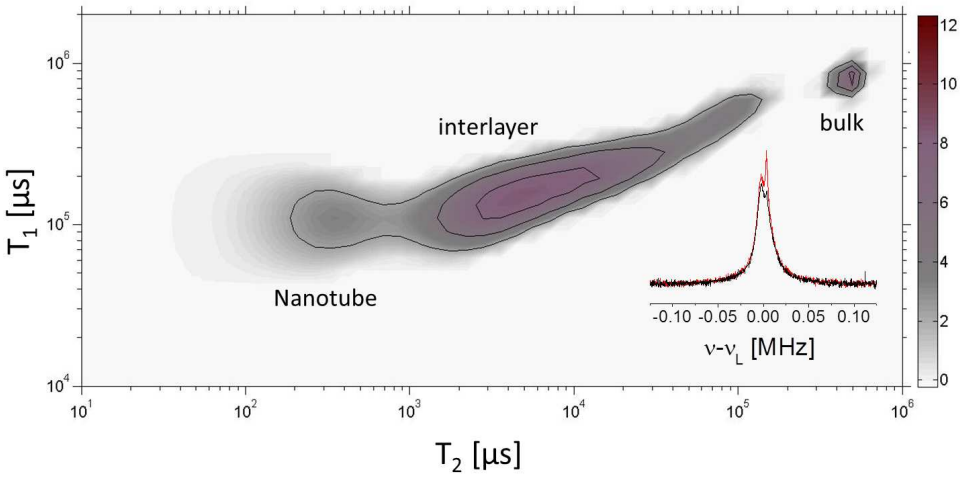

FIG. 6: ^{1}H NMR $T_1 - T_2$ correlation spectroscopy of a water saturated DWCNT at room temperature in the external magnetic field of 9.4 Tesla. The inset shows the corresponding ^{1}H NMR spectrum at repetition times TR=0.5 sec and 5 sec, respectively.

To further enlighten the different kinds of water probed in our NMR experiments, spin-lattice to spin-spin ^{1}H NMR $T_1 - T_2$ correlation spectroscopy was performed at room temperature on a water saturated DWCNT sample, and results are shown in Fig. 6. This type of spectroscopy provides information about the "liquidity" of the local molecular environment: in general, molecules in unconstraint liquid environment are characterized by $T_1 \approx T_2$, whereas molecules in rigid (solid) environment show $T_2 << T_1$. In this context, bulk water with $T_1 \approx T_2$, interstitial water with T_1 moderately higher than T_2, and solid-like nanotube water with $T_2 << T_1$ are clearly visible in Fig. 6. The inset shows the relevant ^{1}H NMR spectra at 400 MHz and at two different repetition times. Two ^{1}H NMR peaks are observed, which are splitted by $\approx$ 2 kHz; a high frequency peak with long T_1 as concluded by the rapid decrease of the signal intensity at short repetition time TD, which is assigned to bulk water, and a low frequency peak with fast relaxation (shorter T_1), which is assigned to interstitial and nanotube water.

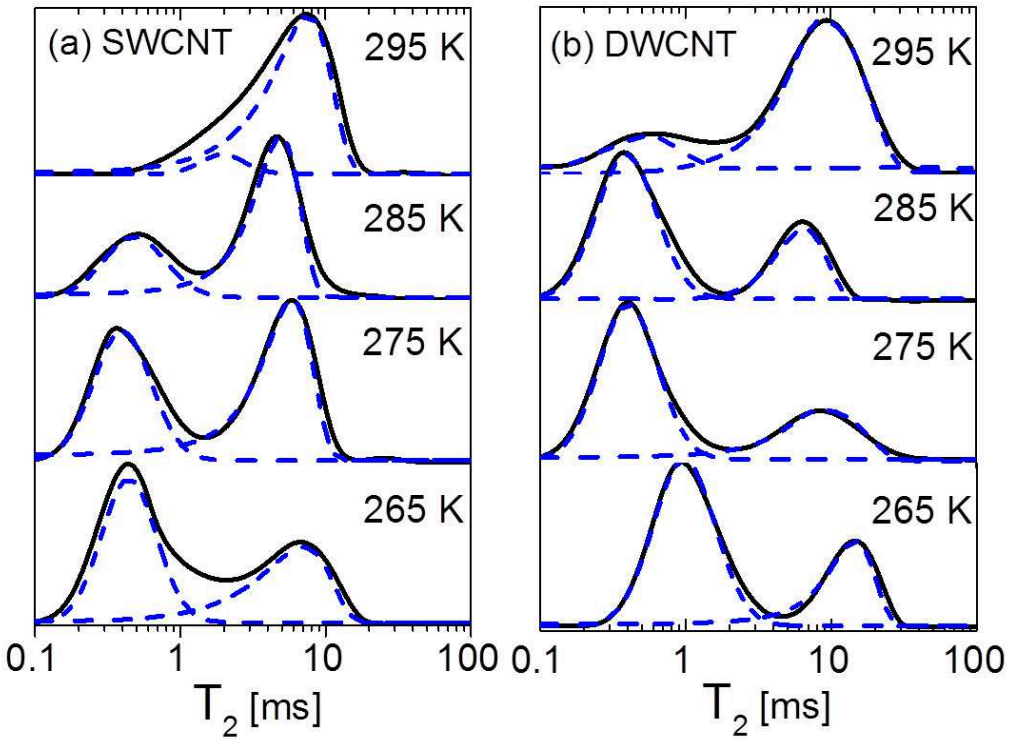

FIG. 7: T_2 projections of the $D-T_2$ spectra of water in (a) SWCNTs and (b) DWCNTs. For clarity, all T_2 projections have been normalized. Fits (dashed lines) were performed with inversion of a stretched exponential spin echo decay and a log-norm distribution of T_2s . The short T_2 component corresponds to the nanotube water and the long T_2 component to the interstitial water. The apparent higher intensity of the short T_2 peak from the nanotube water upon lowering temperature is due to the contribution of the low-D tail, as seen in Figure 2 of the manuscript.

Fig. 7 presents the T_2 projections of $D - T_2$ spectra at selected temperatures for both SWCNT and DWCNT. Each projection consists mainly of two peaks; a short T_2 peak corresponding to the nanotube water, i.e. water in the interior of the CNTs, and a long T_2 component corresponding mainly to the interstitial water.

Most astonishing, in the double-walled CNTs the short T_2 water component shows higher diffusion coefficient D values in comparison to the long T_2 water component, as clearly seen in Figure 4a of the manuscript. A similar surprising result was observed in pulsed gradient diffusion experiments of water in hydrating collagen II [8], where the water fraction with the low diffusion was shown to have longer T_2 and hence higher local mobility, in comparison to the water fraction with the high diffusion, which was shown to have shorter T_2 and hence

reduced local mobility.

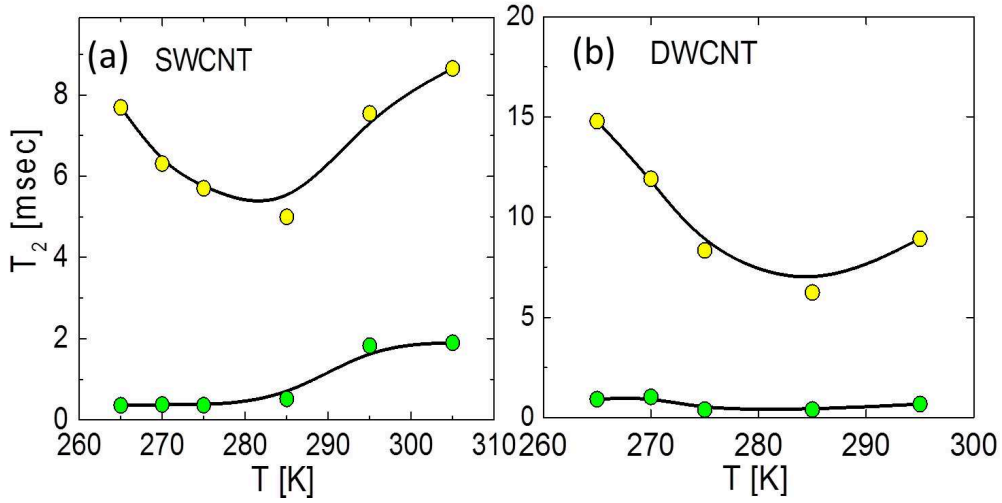

FIG. 8: Temperature dependence of water-T_2 inside a) SWCNT and b) DWCNT samples.

Fig. 8 demonstrates the temperature dependence of the T_2 peak positions for both the SWCNT and DWCNT samples. Upon lowering temperature, the T_2 value of the nanotube water in the SWCNT (green circles in Fig. 8a shifts to lower values, from $\approx$ 2 ms at room temperature to $\approx$0.2 ms at 265 K. In the DWCNTs T_2 of the nanotube water (green circles in Fig. 8b) remains almost constant at about 0.5 ms. In the case of interstitial water (yellow circles), an apparent local minimum at 285 K is observed for both samples, which might be related to the change of hydrophobicity, as discussed in a recent NMR publication [9]. More work is needed to clarify this issue.

* Corresponding author: Jamal.Hassan@kustar.ac.ae

† Corresponding author: g.papavassiliou@inn.demokritos.gr

[1] Kimmich, W. Unrath, G. Schnur, E. Rommel, NMR measurement of small self-diffusion coefficients in the fringe field of superconducting magnets, Journal of Magnetic Resonance **91**, 136-140 (1991).

[2] G. Leu, E.J. Fordham, M.D. H?rlimann, P. Frulla, Fixed and pulsed gradient diffusion methods in low-field core analysis, Magnetic Resonance Imaging **23**, 305-309 (2005).

[3] M.N. d'Eurydice, P. Galvosas, D-T 2 correlation using the inhomogeneity of single sided NMR devices, Microporous and Mesoporous Materials **205**, 40-43 (2005).

[4] M.N. d'Eurydice, P. Galvosas, Measuring diffusion-relaxation correlation maps using non-uniform field gradients of single-sided NMR devices, Journal of Magnetic Resonance **248**, 137-145 (2014).

[5] J. Mitchell, T. Chandrasekera, L. Gladden, Numerical estimation of relaxation and diffusion distributions in two dimensions, Progress in nuclear magnetic resonance spectroscopy **62**, 34-50 (2012).

[6] I.J. Day, On the inversion of diffusion NMR data: Tikhonov regularization and optimal choice of the regularization parameter, Journal of Magnetic Resonanc **211**(2), 178-185 (2011).

[7] P. T. Callaghan, K. W. Jolley, and J. Lelievre, Diffusion of water in the endosperm tissue of wheat grains as studied by pulsed field gradient Nuclear Magnetic Resonance,Biophys. J. **28**, 133-142 (1979).

[8] R. Knauss, G. Fleischer, W. Griinder, J. Karger, A. Werner, Pulsed Field Gradient NMR and Nuclear Magnetic Relaxation Studies of Water Mobility in Hydrated Collagen II, Magnetic Resonance in Medicine **36**, 241-248 (1996).

[9] Hai-Jing Wang, Xue-Kui Xi, Alfred Kleinhammes, Yue Wu, Temperature-Induced Hydrophobic-Hydrophilic Transition Observed by Water Adsorption, Science **322**, 80-83 (2008).